Available online at www.sciencedirect.com
ScienceDirect
Journal of Sound and Vibration 313 (2008) 676–695
JOURNAL OF SOUND AND VIBRATION
www.elsevier.com/locate/jsvi

Wave reflection and transmission in composite beams containing semi-infinite delamination

Wan-Chun Yuan[a], Li Zhou[a], Fuh-Gwo Yuan[b,*]

[a]College of Aerospace Engineering, Nanjing University of Aeronautics & Astronautics, Nanjing 210016, China
[b]Department of Mechanical and Aerospace Engineering, North Carolina State University, Raleigh, NC 27695-7921, USA

Received 26 January 2007; received in revised form 18 November 2007; accepted 3 December 2007
Handling Editor: P. Davies
Available online 8 February 2008

Abstract

Wave reflection and transmission in composite beams containing a semi-infinite delamination is studied analytically based on Timoshenko beam theory. Two extreme cases of delaminated surface conditions: non-contact (open) and fully contact (closed) delaminations, are examined, respectively, for a unidirectional composite beam. Analytical solutions of reflection and transmission coefficients for time harmonic flexural waves in a semi-infinite delaminated beam are obtained. The portion of reflected and transmitted power (energy) depends strongly on the frequency of the incident flexural waves as well as the delamination position. The power reflection and transmission ratios are also calculated and verified through energy conservation. The transmitted energy among various wave modes is also investigated. The interaction of narrowband incident wave with delamination at different positions through the thickness of a composite beam is then studied by analytical analysis and verified by finite element analysis.

1. Introduction

One of the commonly encountered defects or damages in laminated composite structures is delamination. The delamination not only causes reduction in stiffness, but also affects the strength and integrity of the structure, leading to its final failure. The delamination also affects its vibration and stability characteristics of laminated beam type structures. Vibration characteristics of beams containing delamination or inhomogeneity have been investigated analytically and experimentally [1–4]. The vibration characteristics of the delaminated beam, such as natural frequencies and mode shapes, have been examined. As expected, using this passive diagnosis method the change of these modal parameters is insensitive to the extent of the damage for the first few natural frequencies. An active diagnosis method by exciting controlled waves into the structure is used to detect the localized damage. When the incident wave propagates in the beam containing delamination [3,4], the interaction of the incident wave with the delamination induces scattered waves. The scattered waves in the form of reflected and transmitted waves may carry information on the nature of the damage. The guided

*Corresponding author. Tel.: +1 191 951 55947.
E-mail address: yuan@ncsu.edu (F.-G. Yuan).

0022-460X/$ - see front matter © 2007 Elsevier Ltd. All rights reserved.
doi:10.1016/j.jsv.2007.12.012

waves in beams are characterized by their multimodal and dispersive nature. When the guided waves are incident on the discontinuities, mode conversion may occur as a result of satisfying the boundary conditions along the discontinuities. Since such waveguide induces stresses through the beam thickness, the entire thickness of the beam is interrogated, which means that it is possible to determine the depth of the delamination.

Flexural wave propagation in the delaminated beam has also been investigated [5–9], but to a lesser extent. The delamination splits the portion of the beam into two delaminated sub-beams. The transmitted flexural wave velocity in the delaminated region is decreased due to the reduction of overall bending stiffness. Ostachowicz et al. [9] modeled a finite delaminated isotropic beam by spectral finite elements. Additional wave packets shown in acceleration response are induced due to wave reflection from the delamination. However, they did not consider the interaction between the two delaminated sub-beams. None of the studies considered the power transport of transient wave packets, which can be useful for damage identification. Power flow in beam-like structures can be obtained from both theory and experiments [10,11]. To our best knowledge, no relationship between the incident wave and the reflected or transmitted waves has been presented. Bazer and Burridge [12] derived a general solution of power flow of plane waves at an interface in a three-dimensional medium. They are concerned with the energy balance associated with the reflection and refraction of harmonic plane waves governed by the differential equations at a plane interface or boundary. The power flow in the incident wave is equal to the sum of that in the reflected and refraction waves, which indicates the power conservation. Wang and Rose [13] investigated the wave propagation in isotropic beams

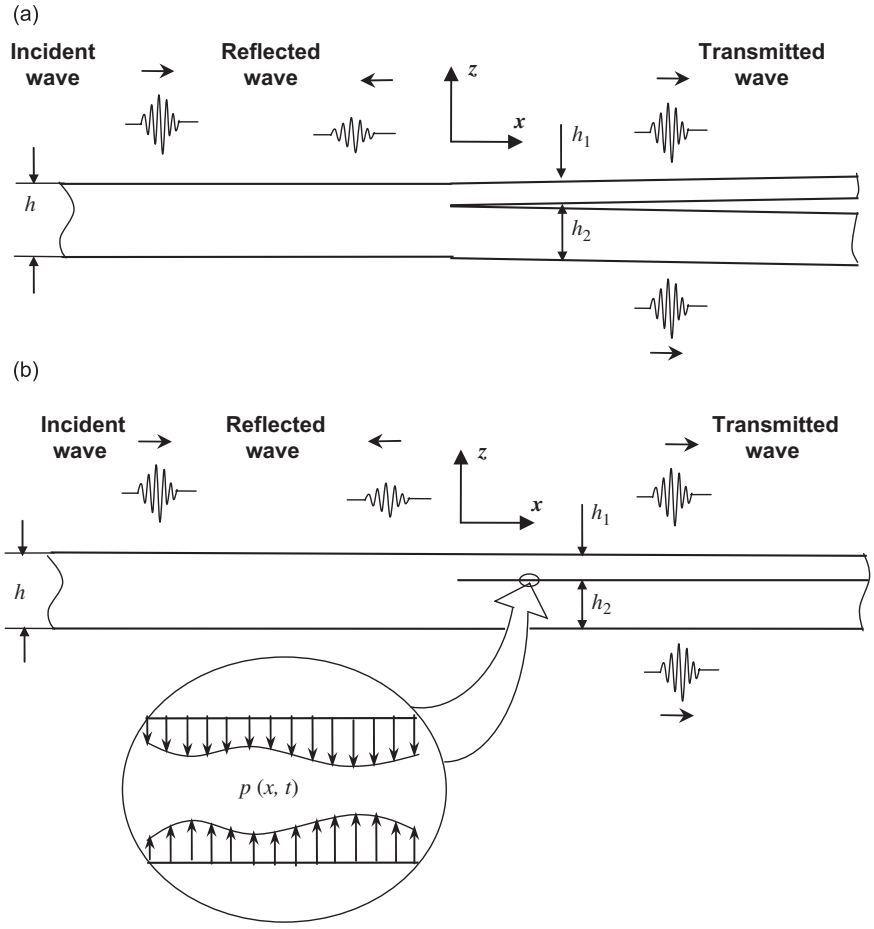

Fig. 1. Reflection and transmission of an incident wave in beams containing semi-infinite delamination: (a) open delamination and (b) closed delamination.

containing semi-infinite delamination. Only the closed delamination is considered and the results of symmetric delamination are given in comparison with the closed delamination modeled by equivalent inhomogeneity.

The purpose of this paper is to present an analytical method for analyzing the wave behavior of the delaminated beam and for determining the (power) reflection from and transmission through a semi-infinite delaminated composite beam. The composite beam is modeled using Timoshenko beam theory. Upon wave incidence on the beam the waveguide propagates toward the delamination, then splits into two waveguides in the delaminated sub-beams, each with its own higher cut-off frequency. The crack surfaces may experience partially closed or open in a time-varying manner. To analytically model the delamination region, two extreme cases signifying the extreme cases of delaminated surface condition during the wave propagation are considered. One is that the delamination surfaces are completely open. It means there is no contact between two sub-beams. The transmitted waves in sub-beams are independent of each other; while the other assumed that the delaminated surfaces are completely closed, that has been discussed in Ref. [13], the surfaces are in contact. These two cases are shown in Fig. 1(a) and (b), respectively. The two cases are described as open and closed delaminations herein.

The paper is organized as follows. Dispersion relation, phase and group velocities of Timoshenko beams are analyzed in Section 2. The reflection and transmission coefficients for the open and closed delaminations are derived, respectively, in Section 3. In Section 4 the power reflection and transmission and power distribution among transmitted wave modes are analyzed. Numerical results are conducted in Section 5. Comparison of results from analytical solutions and finite element method is made in Section 6. Finally conclusions are drawn in Section 7.

2. Dispersion relations of Timoshenko beams

Based on Timoshenko beam theory, the general displacements of the composite beam can be described as

$$U(x,z,t) = u(x,t) + z\psi(x,t), \quad V(x,z,t) = 0, \quad W(x,z,t) = w(x,t), \tag{1}$$

where x-axis is the centroidal axis of the (sub-) beam. $u(x,t)$ is the axial displacement of the beam in the x-direction. $\psi(x,\ t)$ is the rotation of the cross-section of the beam about the y-axis; $w(x,t)$ is the transverse displacement of the beam in the z-direction. The non-vanishing strain components provided by Eq. (1) are

$$\varepsilon_x = u_{,x} + z\psi_{,x}, \quad \gamma_{xz} = w_{,x} + \psi. \tag{2}$$

The equilibrium equations for a symmetric laminated beam [14] can be written as

$$N_{,x} = I_1\ddot{u}, \quad V_{,x} = I_1\ddot{w}, \quad M_{,x} - V = I_2\ddot{\psi}, \tag{3}$$

where

$$N = \int_{-h/2}^{h/2} \sigma_x \,\mathrm{d}z, \quad V = \int_{-h/2}^{h/2} \tau_{xz} \,\mathrm{d}z, \quad M = \int_{-h/2}^{h/2} \sigma_x z \,\mathrm{d}z. \tag{4}$$

N, V, and M are the axial force, shear force, and bending moment per unit beam width of the composite beam; σ_x and τ_{xz} are the axial and shear stresses, respectively, h is the thickness of the beam

$$I_1 = \int_{-h/2}^{h/2} \rho \,\mathrm{d}z \text{ and } I_2 = \int_{-h/2}^{h/2} \rho z^2 \,\mathrm{d}z \tag{5}$$

are the translational and rotational inertia per unit beam width, respectively, and ρ is the mass density of the laminated beam.

For the composite beam, the stiffness of an off-axis composite can be written in the following form [14]:

$$\boldsymbol{C} = \begin{bmatrix} C_{11} & C_{12} & C_{13} & 0 & 0 & C_{16} \\ C_{12} & C_{22} & C_{23} & 0 & 0 & C_{26} \\ C_{13} & C_{23} & C_{33} & 0 & 0 & C_{36} \\ 0 & 0 & 0 & C_{44} & C_{45} & 0 \\ 0 & 0 & 0 & C_{45} & C_{55} & 0 \\ C_{16} & C_{26} & C_{36} & 0 & 0 & C_{66} \end{bmatrix}. \tag{6}$$

Since the transverse shear strain is taken as a constant through the beam thickness, a shear adjustment coefficient κ is introduced such that transverse shear force would be equal to the actual shear force in magnitude. Considering the plane strain in the y-direction (i.e., second equation of Eq. (1)), the constitutive relations between stress and strain can be simplified as

$$\sigma_x = C_{11}\varepsilon_x, \quad \tau_{xz} = \kappa^2 C_{55}\gamma_{xz}, \tag{7}$$

where $\kappa^2 = \pi^2/12$ is the transverse shear correction factor which is determined by the match of the cut-off frequency of the beam theory with that obtained from the Rayleigh–Lamb equation [15]. If the plane stress condition is imposed in the beam, the coefficients of Eq. (7) are replaced by $\tilde{C}_{11} = C_{11} - C_{12}^2/C_{22}$, $\tilde{C}_{55} = C_{55} - C_{45}^2/C_{44}$.

Then the axis force, bending moment, and shear force can be written using Eqs. (4) and (7) by

$$N = A_{11}u_{,x}, \quad M = D_{11}\psi_{,x}, \quad V = \kappa^2 A_{55}(w_{,x} + \psi), \tag{8}$$

where the extensional, shear, and bending stiffnesses are defined by [14]

$$A_{11} = \int_{-h/2}^{h/2} C_{11}\,\mathrm{d}z, \quad A_{55} = \int_{-h/2}^{h/2} C_{55}\,\mathrm{d}z, \quad D_{11} = \int_{-h/2}^{h/2} C_{11}z^2\,\mathrm{d}z. \tag{9}$$

The equilibrium equation given by Eq. (3) can be expressed in terms of displacements as

$$A_{11}u_{,xx} = I_1\ddot{u}, \tag{10a}$$

$$\kappa^2 A_{55}(w_{,xx} + \psi_{,x}) = I_1\ddot{w}, \tag{10b}$$

$$D_{11}\psi_{,xx} - \kappa^2 A_{55}(w_{,x} + \psi) = I_2\ddot{\psi}. \tag{10c}$$

For plane wave solutions the displacements in one-dimensional beam are represented by

$$u = U_0\,\mathrm{e}^{\mathrm{i}(kx-\omega t)}, \quad w = W_0\,\mathrm{e}^{\mathrm{i}(kx-\omega t)}, \quad \psi = \Psi_0\,\mathrm{e}^{\mathrm{i}(kx-\omega t)}. \tag{11}$$

The dispersion relation of flexural waves can be expressed *via* Eqs. (10b) and (10c) as follows:

$$(\kappa^2 A_{55}k^2 - I_1\omega^2)(D_{11}k^2 + \kappa^2 A_{55} - I_2\omega^2) - \kappa^4 A_{55}^2 k^2 = 0. \tag{12}$$

There are four roots of Eq. (12):

$$k_j = \left[\frac{1}{2}\left(1 + \frac{c_l^2}{\kappa^2 c_s^2}\right) \pm \sqrt{\left(\frac{c_l}{q\omega}\right)^2 + \frac{1}{4}\left(1 - \frac{c_l^2}{\kappa^2 c_s^2}\right)^2}\right]^{1/2} \frac{\omega}{c_l} \tag{13}$$

for ($j = 1,2$) and noting $k_3 = -k_1$, $k_4 = -k_2$,

In Eq. (13) $c_s = \sqrt{A_{55}/I_1}$ and $c_l = \sqrt{D_{11}/I_2}$ are shear and plate wave velocities, respectively. For a unidirectional composite beam with rectangular cross-section, these velocities are independent of beam thickness and $q = \sqrt{I_2/I_1} = h/\sqrt{12}$.

Using the following non-dimensional variables,

$$\begin{aligned} &\overline{x} = x/h, \quad \overline{w} = w/h, \\ &\overline{t} = t/\tau, \quad \overline{k} = kh, \quad \overline{\omega} = \omega\tau, \end{aligned} \tag{14}$$

where the reference length scale is the thickness of the (sub-)beam h and a typical time scale $\tau = h/c_s$, the resulting non-dimensional dispersion relation is

$$\overline{k}_j = \left[\frac{(\alpha+\kappa^2)}{2\alpha\kappa^2} \pm \sqrt{\frac{12}{\alpha\overline{\omega}^2} + \frac{1}{4}\left(\frac{1}{\alpha}-\frac{1}{\kappa^2}\right)^2}\right]^{1/2} \overline{\omega}\,(j=1,2), \quad \overline{k}_3 = -\overline{k}_1, \quad \overline{k}_4 = -\overline{k}_2, \tag{15}$$

where $\alpha = (c_l/c_s)^2$.

The cut-off frequency of the A_1 mode can be simply determined by setting $k_2 = 0$ in Eq. (13), which gives

$$\omega_c = \kappa c_s/q. \tag{16}$$

Phase velocities and group velocities are given by

$$c_p = \omega/k, \quad c_g = \mathrm{d}\omega/\mathrm{d}k. \tag{17}$$

When frequencies approach infinity, the wave velocity becomes non-dispersive. According to Eqs. (13) and (17), the phase and group velocities of two flexural modes can be simply derived

$$c_{g0} = \kappa c_s, \quad c_{g1} = c_l \ \text{ as } \ \omega \to \infty.$$

Clearly these two group velocities do not depend on the thickness of the beam.

In the relatively low frequency range, $\omega < \omega_c$, the Timoshenko beam experiences a pair of propagating waves (one positive-going and one negative-going) plus two evanescent (near-field) waves, the value of k being purely imaginary. The pair of propagating waves is called the lowest fundamental flexural A_0 wave modes. These two near-field waves can be regarded as positive- and negative-going attenuating waves which decay exponentially with the wave travel distance. Beyond the cut-off frequency ω_c, two pairs of propagating waves (two positive-going and two negative-going) co-exist, called A_0 and A_1 modes. Thus, with an increase of frequency, a non-propagating mode can decay more slowly and eventually becomes a propagating mode.

A general solution of Eq. (10b) and Eq. (10c) is given by

$$w(x,t) = \sum_{j=1}^{4} a_j\, \mathrm{e}^{\mathrm{i}(k_j x-\omega t)}, \quad \psi(x,t) = \sum_{j=1}^{4} F_j a_j\, \mathrm{e}^{\mathrm{i}(k_j x-\omega t)}, \tag{18}$$

where $F_j = \mathrm{i}[(\omega/\kappa c_s)^2 - k_j^2]/k_j$ $(j=1,2)$, $F_3 = -F_1$ and $F_4 = -F_2$. The amplitudes a_j may be complex.

For the extensional wave mode governed by Eq. (10a), there exists a pair of propagating waves (one positive-going and negative-going). The wave is non-dispersive based on the Timoshenko beam theory whose dispersion relation is given by

$$k_e = \sqrt{I_1/A_{11}}\,\omega. \tag{19}$$

3. Reflection and transmission matrices

When a propagating time harmonic wave is incident upon a discontinuity, it is scattered into waves reflected from and transmitted through the discontinuity whose magnitudes and phases can be quantified by reflection and transmission matrices. The total wave field can be expressed as a sum of the incident wave field and the scattered wave field. The mode incident on the delamination results in both reflected and transmitted waves of all orders of the wave modes that could exist in the beam for a given frequency. It is assumed that far away from the discontinuity the reflected and transmitted waves are plane waves. The incident time harmonic wave induces not only propagating waves (real wavenumber) and non-propagating evanescent near-field waves (purely imaginary wavenumber). In this section, a propagating flexural wave at far-field excited on a unidirectional composite beam incident upon a semi-infinite delamination is studied. The far field is defined here as the distance where the contribution of non-propagating wave can be neglected. Two extreme cases of delaminated surface conditions: non-contact (open) and fully contact (closed) delaminations, are considered, respectively. The reflection and transmission matrices of both open and closed delaminations are derived separately.

3.1. Open delamination

Consider a slender beam containing a semi-infinite delamination shown in Fig. 1(a), the origin of the coordinate is located at the tip of the delamination. The beam can be divided into two regions. The left region is the un-delaminated region which contains both incident and reflected waves; while the right region encompasses the two delaminated sub-beams. Since the delamination surfaces are open, there is no contact pressure between the surfaces. Only positive-going wave exists in the two sub-beams, which refers to the transmitted wave.

Considering an incident flexural wave traveling in the positive x-direction, in the left un-delaminated region ($x \leqslant 0$) when the excitation frequency is greater than the cut-off frequency, the wave fields consist of two positive-going incident flexural waves and two negative-going reflected flexural waves that can be written as

$$w_0 = a\,\mathrm{e}^{\mathrm{i}k_1 x} + b\,\mathrm{e}^{\mathrm{i}k_2 x} + a_r\,\mathrm{e}^{-\mathrm{i}k_1 x} + b_r\,\mathrm{e}^{-\mathrm{i}k_2 x}, \tag{20a}$$

$$\psi_0 = F_1 a\,\mathrm{e}^{\mathrm{i}k_1 x} + F_2 b\,\mathrm{e}^{\mathrm{i}k_2 x} - F_1 a_r\,\mathrm{e}^{-\mathrm{i}k_1 x} - F_2 b_r\,\mathrm{e}^{-\mathrm{i}k_2 x}. \tag{20b}$$

Due to the moment continuity on the junction, an induced extensional wave may also be reflected from the discontinuity and transmitted into two sub-beams. The negative-going reflected extensional wave in the left region can be expressed as

$$u_0 = c_r\,\mathrm{e}^{-\mathrm{i}k_e x}, \tag{20c}$$

where the time dependence term $\mathrm{e}^{-\mathrm{i}\omega t}$ has been suppressed here and hereafter. When the excitation frequency is below the cut-off frequency, i.e., $\omega < \omega_c$, the second pair wave mode becomes evanescent since the wavenumber k_2 is purely imaginary. The choice of the sign in k_2 is dictated by the condition that the reflected wave field is finite as $x \to -\infty$. In this case, the sign of k_2 is deliberately chosen to be negative. The coefficients of a and b represents the amplitude of incident wave depending on the details of the loading away from the discontinuity. When excited at far field in the low frequency b can be set to zero. In the limit when frequency approaches infinity, the group velocities of the two modes are given by Eq. (17).

In the right delaminated region ($x \geqslant 0$) where the crack surfaces are completely open, the displacements of the two independent sub-beams are denoted by u_1, w_1, ψ_1, u_2, w_2, ψ_2. The subscripts 1 and 2 denote the upper and lower sub-beams, respectively. Since waves are transmitted from the incident waves through the discontinuity, the general solutions of displacement for the transmitted waves in each sub-beam are given by

$$w_n = a_t^{(n)}\,\mathrm{e}^{\mathrm{i}k_1^{(n)} x} + b_t^{(n)}\,\mathrm{e}^{\mathrm{i}k_2^{(n)} x}, \tag{21a}$$

$$\psi_n = F_1^{(n)} a_t^{(n)}\,\mathrm{e}^{\mathrm{i}k_1^{(n)} x} + F_2^{(n)} b_t^{(n)}\,\mathrm{e}^{\mathrm{i}k_2^{(n)} x} \quad (n = 1, 2), \tag{21b}$$

$$u_n = c_t^{(n)}\,\mathrm{e}^{\mathrm{i}k_e^{(n)} x}, \tag{21c}$$

where superscripts (1) and (2) denote the parameters associated with each sub-beam. The wavenumber $k_j^{(n)}$ and $F_j^{(n)}$can be readily obtained by substituting the stiffness and moment of inertia pertaining to the each sub-beam in Eqs. (4), (5) and (9). According to Eq. (19), the wavenumber of the extensional wave is independent of beam thickness implying $k_e = k_e^{(1)} = k_e^{(2)}$.

The cut-off frequency of each sub-beam can be written as follows:

$$\omega_c^{(1)} = \kappa c_s / q^{(1)}, \quad \omega_c^{(2)} = \kappa c_s / q^{(2)}, \tag{22}$$

where $q^{(n)} = \sqrt{I_2^{(n)}/I_1^{(n)}}$ $(n = 1,2)$.

The group velocities of two flexural wave modes in each sub-beam at infinite frequency, according to Eq. (17), are

$$c_{g0}^{(n)d} = \kappa c_s, \quad c_{g1}^{(n)d} = c_l \ \text{ as } \ \omega \to \infty \quad (n = 1, 2), \tag{23}$$

where the superscript d denotes the delaminated beams.

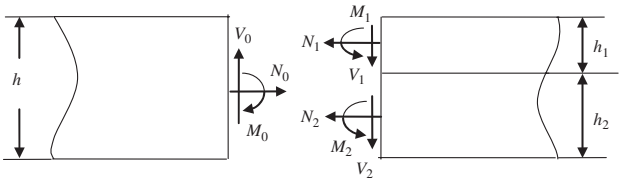

Fig. 2. Free body diagram of delaminated beam.

The amplitudes of these waves involving nine unknowns (a_r, b_r, c_r, $a_t^{(1)}$, $b_t^{(1)}$, $c_t^{(1)}$, $a_t^{(2)}$, $b_t^{(2)}$, $c_t^{(2)}$) can be determined from the following continuity and equilibrium conditions at the junction, $x = 0$ as shown in Fig. 2

$$w_0 = w_1 = w_2, \quad \psi_0 = \psi_1 = \psi_2, \quad u_1 = u_0 + \frac{h_2}{2}\psi_0, \quad u_2 = u_0 - \frac{h_1}{2}\psi_0,$$
$$N_0 = N_1 + N_2, \quad M_0 = M_1 + M_2 + \frac{h_2}{2}N_1 - \frac{h_1}{2}N_2, \quad V_0 = V_1 + V_2. \tag{24}$$

Substituting Eqs. (20) and (21) together with Eq. (8) into Eq. (24) leads to the following matrix form:

$$\begin{bmatrix} -1 & -1 & 0 & 1 & 1 & 0 & 0 & 0 & 0 \\ -1 & -1 & 0 & 0 & 0 & 0 & 1 & 1 & 0 \\ F_1 & F_2 & 0 & F_1^{(1)} & F_2^{(1)} & 0 & 0 & 0 & 0 \\ F_1 & F_2 & 0 & 0 & 0 & 0 & F_1^{(2)} & F_2^{(2)} & 0 \\ F_1h_2 & F_2h_2 & -2 & 0 & 0 & 2 & 0 & 0 & 0 \\ F_1h_1 & F_2h_1 & 2 & 0 & 0 & 0 & 0 & 0 & -2 \\ 0 & 0 & h & 0 & 0 & h_1 & 0 & 0 & h_2 \\ -k_1F_1 & -k_2F_2 & 0 & \alpha_1^{(1)} & \alpha_2^{(1)} & \beta & \alpha_1^{(2)} & \alpha_2^{(2)} & -\beta \\ \gamma_1 & \gamma_2 & 0 & \gamma_1^{(1)} & \gamma_2^{(1)} & 0 & \gamma_1^{(2)} & \gamma_2^{(2)} & 0 \end{bmatrix} \begin{bmatrix} a_r \\ b_r \\ c_r \\ a_t^{(1)} \\ b_t^{(1)} \\ c_t^{(1)} \\ a_t^{(2)} \\ b_t^{(2)} \\ c_t^{(2)} \end{bmatrix} = \begin{bmatrix} 1 & 1 \\ 1 & 1 \\ F_1 & F_2 \\ F_1 & F_2 \\ F_1h_2 & F_2h_2 \\ F_1h_1 & F_2h_1 \\ 0 & 0 \\ k_1F_1 & k_2F_2 \\ \gamma_1 & \gamma_2 \end{bmatrix} \begin{bmatrix} a \\ b \end{bmatrix}, \tag{25}$$

where $\alpha_m^{(n)} = k_m^{(n)} F_m^{(n)} (h_n/h)^3$, $\beta = 6(h_1h_2/h^3)k_e$, $\gamma_m{}^{(n)} = h_n(\mathrm{i}k_m{}^{(n)} + F_m{}^{(n)})$, $m, n = 1,2$.

The coefficients of reflected and transmitted waves can be symbolically represented in terms of the coefficients of the incident wave in the following relation:

$$[a_r, b_r, c_r]^{\mathrm{T}} = \mathbf{R}_{3\times2}[a, b]^{\mathrm{T}}, \tag{26a}$$

$$[a_t^{(1)}, b_t^{(1)}, c_t^{(1)}]^{\mathrm{T}} = \mathbf{T}_{3\times2}^{(1)}[a, b]^{\mathrm{T}}, \tag{26b}$$

$$[a_t^{(2)}, b_t^{(2)}, c_t^{(2)}]^{\mathrm{T}} = \mathbf{T}_{3\times2}^{(2)}[a, b]^{\mathrm{T}}, \tag{26c}$$

where $\mathbf{R}_{3\times2}$, $\mathbf{T}_{3\times2}^{(1)}$, and $\mathbf{T}_{3\times2}^{(2)}$ denote reflection and the transmission matrices whose components are complex in general. For example, in reflection matrix $\mathbf{R}_{3\times2}$ the component R_{12} means the second incident flexural wave mode converts into the first reflected flexural mode from the discontinuity. Similarly, the transmitted mode conversion also occurs. The extensional wave mode may be induced in the composite beam. This means the flexural wave will partly transform to the extensional mode when the incident wave is reflected from the delamination tip or transmitted into the delaminated region. The proportion of the extensional mode conversion compared with the flexural mode conversion depends on the incident wave frequency and position of the delamination in the thickness direction. This will be discussed in detail in Section 5.

3.2. Closed delamination

The displacements of the left un-delaminated region are the same as in the open delamination case. Denoting the contact pressure between the two delaminated surfaces as $p(x, t)$, as shown in Fig. 1(b), with the identical transverse displacement, i.e., $\hat{w} = w_1 = w_2$, the following governing equations of flexural wave can be

derived:

$$\kappa^2 A_{55}^{(1)}(\hat{w}_{,xx}+\psi_{1,x}) = I_1^{(1)}\ddot{\hat{w}} + p, \tag{27a}$$

$$D_{11}^{(1)}\psi_{1,xx} - \kappa^2 A_{55}^{(1)}(\hat{w}_{,x}+\psi_1) = I_2^{(1)}\ddot{\psi}_1, \tag{27b}$$

$$\kappa^2 A_{55}^{(2)}(\hat{w}_{,xx}+\psi_{2,x}) = I_1^{(2)}\ddot{\hat{w}} - p, \tag{27c}$$

$$D_{11}^{(2)}\psi_{2,xx} - \kappa^2 A_{55}^{(2)}(\hat{w}_{,x}+\psi_2) = I_2^{(2)}\ddot{\psi}_2. \tag{27d}$$

The contact pressure p can be eliminated by combining Eqs. (27a) and (27c), to obtain

$$\kappa^2(A_{55}\hat{w}_{,xx} + A_{55}^{(1)}\psi_{1,x} + A_{55}^{(2)}\psi_{2,x}) = I_1\ddot{\hat{w}}. \tag{28}$$

If the displacements are introduced as

$$\hat{w} = \hat{W}\,\mathrm{e}^{\mathrm{i}(\hat{k}x-\omega t)}, \quad \psi_1 = \Psi_1\,\mathrm{e}^{\mathrm{i}(\hat{k}x-\omega t)}, \quad \psi_2 = \Psi_2\,\mathrm{e}^{\mathrm{i}(\hat{k}x-\omega t)}. \tag{29}$$

Then by substitution of Eq. (29) into Eqs. (28), (27b), and (27d), the dispersion relation can be determined as follows:

$$\det\left\{\begin{bmatrix} \kappa^2 A_{55}\hat{k}^2 & -\mathrm{i}\kappa^2 A_{55}^{(1)}\hat{k} & -\mathrm{i}\kappa^2 A_{55}^{(2)}\hat{k} \\ \mathrm{i}\kappa^2 A_{55}^{(1)}\hat{k} & D_{11}^{(1)}\hat{k}^2 + \kappa^2 A_{55}^{(1)} & 0 \\ \mathrm{i}\kappa^2 A_{55}^{(2)}\hat{k} & 0 & D_{11}^{(2)}\hat{k}^2 + \kappa^2 A_{55}^{(2)} \end{bmatrix} - \omega^2 \begin{bmatrix} I_1 & 0 & 0 \\ 0 & I_2^{(1)} & 0 \\ 0 & 0 & I_2^{(2)} \end{bmatrix}\right\} = 0. \tag{30}$$

The results give rise to three flexural wave modes. Loosely these modes can be related to the fundamental flexural mode of the un-delaminated portion of the beam, $A_0^{(0)d}$, and the other two related to the A_1 mode in the upper and lower sub-beams, $A_1^{(1)d}$ and $A_1^{(2)d}$, respectively. Two cut-off frequencies can be readily proved to be identical to those in the open delaminating case. When the frequencies approach infinity, according to Eqs. (30) and (17), the group velocities of the three flexural modes can be exactly derived

$$c_{g0}^{(0)d} = \kappa c_s, \quad c_{g1}^{(1)d} = c_{g1}^{(2)d} = c_l \text{ as } \omega \to \infty. \tag{31}$$

The general solution of the positive-going transmitted flexural waves in the delaminated region can be conveniently written as

$$\hat{w} = a_t\,\mathrm{e}^{\mathrm{i}\hat{k}_0 x} + b_t^{(1)}\,\mathrm{e}^{\mathrm{i}\hat{k}_1 x} + b_t^{(2)}\,\mathrm{e}^{\mathrm{i}\hat{k}_2 x}, \tag{32a}$$

$$\psi_n = G_0^{(n)} a_t\,\mathrm{e}^{\mathrm{i}\hat{k}_0 x} + G_1^{(n)} b_t^{(1)}\,\mathrm{e}^{\mathrm{i}\hat{k}_1 x} + G_2^{(n)} b_t^{(2)}\,\mathrm{e}^{\mathrm{i}\hat{k}_2 x} \ \ (n=1,2), \tag{32b}$$

where $G_j^{(n)} = (\mathrm{i}\hat{k}_j/[(\omega q^{(n)})/(\kappa c_s^{(n)})]^2 - [q^{(n)}(\hat{k}_j/\kappa)(c_l^{(n)}/c_s^{(n)})]^2 - 1)$, ($n$ = 1,2 and j = 0,1,2).

The extensional waves in the two sub-beams are the same as in the open delamination case. There are a total of eight amplitudes (a_r, b_r, c_r, a_t, $b_t^{(1)}$, $b_t^{(2)}$, $c_t^{(1)}$, $c_t^{(2)}$) which can be determined from the following continuity and equilibrium conditions at $x = 0$.

$$\begin{aligned} &w_0 = \hat{w}, \quad \psi_0 = \psi_1 = \psi_2, \quad u_1 = u_0 + \frac{h_2}{2}\psi_0, \quad u_2 = u_0 - \frac{h_1}{2}\psi_0, \\ &N_0 = N_1 + N_2, \quad M_0 = M_1 + M_2 + \frac{h_2}{2}N_1 - \frac{h_1}{2}N_2, \quad V_0 = V_1 + V_2. \end{aligned} \tag{33}$$

Substituting Eqs. (20) and (32) together with Eq. (8) into Eq. (33), the equations can be written in matrix form:

$$\begin{bmatrix} -1 & -1 & 0 & 1 & 1 & 1 & 0 & 0 \\ F_1 & F_2 & 0 & G_0^{(1)} & G_1^{(1)} & G_2^{(1)} & 0 & 0 \\ F_1 & F_2 & 0 & G_0^{(2)} & G_1^{(2)} & G_2^{(2)} & 0 & 0 \\ F_1h_2 & F_2h_2 & -2 & 0 & 0 & 0 & 2 & 0 \\ F_1h_1 & F_2h_1 & 2 & 0 & 0 & 0 & 0 & -2 \\ 0 & 0 & h & 0 & 0 & 0 & h_1 & h_2 \\ -k_1F_1 & -k_2F_2 & 0 & \upsilon_0 & \upsilon_1 & \upsilon_2 & \beta & -\beta \\ \gamma_1 & \gamma_2 & 0 & \nu_0 & \nu_1 & \nu_2 & 0 & 0 \end{bmatrix} \begin{bmatrix} a_r \\ b_r \\ c_r \\ a_t \\ b_t^{(1)} \\ b_t^{(2)} \\ c_t^{(1)} \\ c_t^{(2)} \end{bmatrix} = \begin{bmatrix} 1 & 1 \\ F_1 & F_2 \\ F_1 & F_2 \\ F_1h_2 & F_2h_2 \\ F_1h_1 & F_2h_1 \\ 0 & 0 \\ k_1F_1 & k_2F_2 \\ \gamma_1 & \gamma_2 \end{bmatrix} \begin{bmatrix} a \\ b \end{bmatrix}, \tag{34}$$

where $\upsilon_j = \hat{k}_j(G_j^{(1)}(h_1/h)^3 + G_j^{(2)}(h_2/h)^3)$, $\nu_j = h_1(\mathrm{i}\hat{k}_j + G_j^{(1)}) + h_2(\mathrm{i}\hat{k}_j + G_j^{(2)})$ $(j = 0,1,2)$. The reflected and transmitted waves are related to those of incident wave via the following relation:

$$[a_r, b_r, c_r]^{\mathrm{T}} = \mathbf{R}_{3\times2}[a, b]^{\mathrm{T}}, \tag{35a}$$

$$[a_t, b_t^{(1)}, b_t^{(2)}, c_t^{(1)}, c_t^{(2)}]^{\mathrm{T}} = \mathbf{T}_{5\times2}[a, b]^{\mathrm{T}}, \tag{35b}$$

where $\mathbf{R}_{3\times2}$ and $\mathbf{T}_{5\times2}$ denote reflection and transmission matrices, respectively. For fully contacted delaminated surfaces, the transmission matrix contains three coupled flexural modes and two extensional modes in two sub-beams, respectively. The constant pressure distribution p from Eq. (27a) or (27c) indicates the pressure reverses its sign over the delaminated region, implying that the delaminated surfaces may be partially open or closed.

4. Power reflection and transmission

The wave continuously carries energy as it propagates, the rate of energy transport into one end of a cross-section of the beam being, on average, equal to the rate out of the other end of the cross-section if no energy dissipation is involved. This speed of transport, or power flow, is given by the rate of work of internal forces and moments acting on a beam cross-section. A useful representation of the intensity of wave can be represented by an average of power P over time. Over a period t_0, the time-averaged power flow $\langle P \rangle$ per unit beam width in Timoshenko beam is given by

$$\langle P \rangle = -\frac{1}{t_0}\int_0^{t_0} (V\dot{w} + M\dot{\psi} + N\dot{u})\,\mathrm{d}t, \tag{36}$$

where $t_0 = 2\pi/\omega$. Both incident and reflected waves exist in the un-delaminated region. Since only flexural wave is excited at the far field. The third term of Eq. (36) associated with extensional wave vanishes.

Substituting Eqs. (20a) and (20b) together with the force–displacement relations Eq. (8) into Eq. (36), the time-averaged power flow of the incident wave over a cycle can be written as

$$\langle P_i \rangle = \lambda_1|a|^2 + \lambda_2|b|^2 H(\omega - \omega_c), \tag{37}$$

where $\lambda_m = \frac{1}{2}\omega[\kappa^2 A_{55}k_m + D_{11}k_m|F_m|^2 + \kappa^2 A_{55}\,\mathrm{Im}(F_m)]$, $m = 1, 2$. The Heaviside function H used signifies that the term associated with evanescent wave does not carry energy when $\omega < \omega_c$. In this case, only the first term of Eq. (37) remains.

For the reflected wave in un-delaminated region, the total power flow of reflected wave can be written as follows:

$$\langle P_r \rangle = \lambda_1|a_r|^2 + \lambda_2|b_r|^2 H(\omega - \omega_c) + \lambda_e|c_r|^2, \tag{38}$$

where $\lambda_e = \frac{1}{2}\omega k_e A_{11}$.

For a semi-infinite delamination, the incident waves transmit waves into delaminated regions. In the open delaminated surfaces, each sub-beam can be considered as a separate single beam with its own stiffness and

thickness. Thus, power flow of transmitted waves in the open delaminated region can be expressed as

$$\langle P_t\rangle_{\text{open}}^{(n)} = \lambda_1^{(n)}\left|a_t^{(n)}\right|^2 + \lambda_2^{(n)}\left|b_t^{(n)}\right|^2 H(\omega-\omega_c^{(n)}) + \lambda_e^{(n)}\left|c_t^{(n)}\right|^2 \quad (n=1,2), \tag{39}$$

where $\lambda_m^{(n)} = \frac{1}{2}\omega[\kappa^2 A_{55}^{(n)} k_m^{(n)} + D_{11}^{(n)} k_m^{(n)}\left|F_m^{(n)}\right|^2 + \kappa^2 A_{55}^{(n)}\text{Im}(F_m^{(n)})]$, $\lambda_e^{(n)} = \frac{1}{2}\omega k_e A_{11}^{(n)}$, m, n = 1,2.

The superscripts (1) and (2) denote the two separated sub-beams in the open delaminated region.

In the closed delaminated region, two sub-beams are constrained with identical transverse displacement. Similarly the power flow of transmitted wave in the closed delaminated region can be written as follows:

$$\langle P_t\rangle_{\text{closed}}^{(n)} = \eta_0^{(n)}|a_t|^2 + \eta_1^{(n)}\left|b_t^{(1)}\right|^2 H(\omega-\omega_c^{(1)}) + \eta_2^{(n)}\left|b_t^{(2)}\right|^2 H(\omega-\omega_c^{(2)}) + \lambda_e^{(n)}\left|c_t^{(n)}\right|^2, \tag{40}$$

where $\eta_j^{(n)} = \frac{1}{2}\omega[\kappa^2 A_{55}^{(n)}\hat{k}_j + \hat{k}_j D_{11}^{(n)}\left|G_j^{(n)}\right|^2 + \kappa^2 A_{55}^{(n)}\,\text{Im}\,(G_j^{(n)})]$ (n = 1,2, j = 0,1,2).

The superscripts (1) and (2) denote the two coupled sub-beams in the closed delaminated region.

The ratios of the reflected and transmitted power (energy) to the incident energy are defined as

$$R = \frac{\langle P_r\rangle}{\langle P_i\rangle}, \quad T_{\text{open}}^{(n)} = \frac{\langle P_t\rangle_{\text{open}}^{(n)}}{\langle P_i\rangle}, \quad T_{\text{closed}}^{(n)} = \frac{\langle P_t\rangle_{\text{closed}}^{(n)}}{\langle P_i\rangle} \quad (n=1,2). \tag{41}$$

The energy conservation implies

$$R + \sum_{n=1}^{2} T^{(n)} = 1. \tag{42}$$

For transmitted waves in the delaminated region, power (energy) ratios associated with each wave mode can be described as:

$$\begin{aligned}
T_{\text{open}}^{A_0} &= \frac{\lambda_1^{(1)}\left|a_t^{(1)}\right|^2 + \lambda_1^{(2)}\left|a_t^{(2)}\right|^2}{\langle P_t\rangle_{\text{open}}^{(1)} + \langle P_t\rangle_{\text{open}}^{(2)}}, \quad T_{\text{open}}^{A_1} = \frac{\lambda_2^{(1)}\left|b_t^{(1)}\right|^2 + \lambda_2^{(2)}\left|b_t^{(2)}\right|^2}{\langle P_t\rangle_{\text{open}}^{(1)} + \langle P_t\rangle_{\text{open}}^{(2)}}, \quad T_{\text{open}}^{S_0} = \frac{\lambda_e^{(1)}\left|c_t^{(1)}\right|^2 + \lambda_e^{(2)}\left|c_t^{(2)}\right|^2}{\langle P_t\rangle_{\text{open}}^{(1)} + \langle P_t\rangle_{\text{open}}^{(2)}},\\
T_{\text{closed}}^{A_0} &= \frac{\left(\eta_0^{(1)} + \eta_0^{(2)}\right)|a_t|^2}{\langle P_t\rangle_{\text{closed}}^{(1)} + \langle P_t\rangle_{\text{closed}}^{(2)}}, \quad T_{\text{closed}}^{A_1} = \frac{(\eta_1^{(1)} + \eta_1^{(2)})\left|b_t^{(1)}\right|^2 + (\eta_2^{(1)} + \eta_2^{(2)})\left|b_t^{(2)}\right|^2}{\langle P_t\rangle_{\text{closed}}^{(1)} + \langle P_t\rangle_{\text{closed}}^{(2)}},\\
T_{\text{closed}}^{S_0} &= \frac{\lambda_e^{(1)}\left|c_t^{(1)}\right|^2 + \lambda_e^{(2)}\left|c_t^{(2)}\right|^2}{\langle P_t\rangle_{\text{closed}}^{(1)} + \langle P_t\rangle_{\text{closed}}^{(2)}},
\end{aligned} \tag{43}$$

where the superscripts A_0, A_1, S_0 denote the term related to different propagating modes.

5. Numerical results

A unidirectional composite beam made of IM7/5250-4 graphite/epoxy material is chosen as an example in this section. The fibers are aligned with the beam axis and beam cross-section is rectangular. The material properties of the composite are shown in Table 1.

For the composite beam where the delaminated surfaces are modeled to be open, the group velocities of sub-beams and their own cut-off frequencies can be readily determined by Eqs. (14)–(16) using pertaining geometries in each sub-beam. In contrast, the composite beam where delaminated surfaces are completely closed, the group velocities of closed delaminated regions given by Eq. (30) are compared with those from the

Table 1
Material properties of IM7/5250-4 composite

E_L (GPa)	E_T (GPa)	G_{LT} (Gpa)	G_{TZ} (GPa)	v_{LT}	v_{TZ}	ρ (kg/m^3)
168	9.31	5.17	3.45	0.33	0.4	1.61

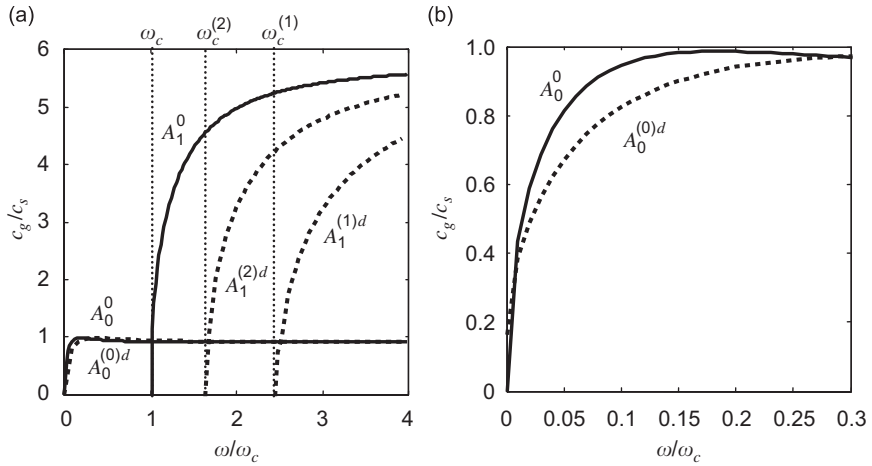

Fig. 3. Group velocities of flexural modes in both un-delaminated region (A_0^0, A_1^0) and closed delaminated region ($A_0^{(0)d}$, $A_1^{(1)d}$, $A_1^{(2)d}$), solid line: un-delaminated region; dotted line: closed delaminated region. (a) All flexural wave modes and (b) close-up view of A_0 modes in the lower frequency domain.

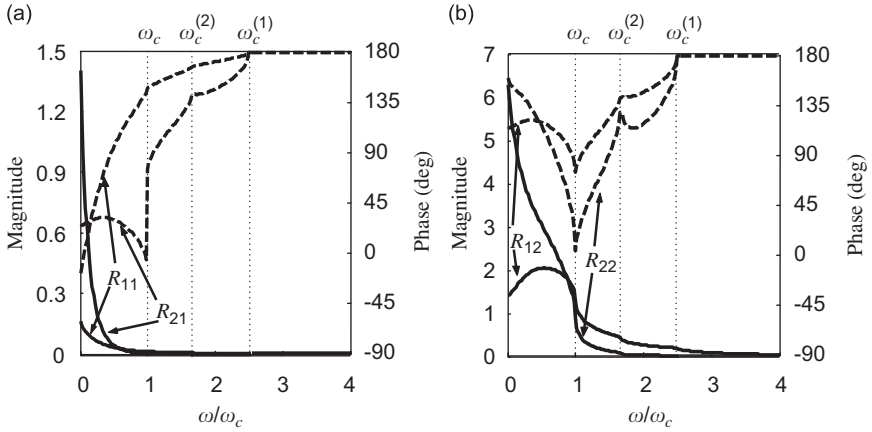

Fig. 4. Reflection coefficients (R_{jk}, for j, $k = 1,2$) at $h_1/h = 0.4$ under open delamination condition (solid line: magnitude; dotted line: phase). Wave reflection from (a) first flexural mode and (b) second flexural mode.

un-delaminated given by Eq. (13), shown in Fig. 3. In this figure, the delamination is located at $h_1/h = 0.4$. The superscripts 0 and d in the figure denote the un-delaminated and delaminated region of the beam, respectively. It can be concluded from Fig. 3(a) that the group velocity curves of two A_0 modes are very close in the whole frequency domain. However, there is a slightly lower group velocities of A_0 mode in the closed delaminated region compared with those in the un-delaminated region when the frequencies are below $0.3\omega_c$, which can be seen in Fig. 3(b). It is mainly due to the reduction of the bending stiffness in the delaminated region. In addition, both A_0 modes tend to reach transverse wave velocity multiplied by the shear correction factor (κc_s) as the frequency approaches infinity. Additional two flexural modes in the closed delaminated region associated with each sub-beam region appear. Their cut-off frequencies are greater than that in the un-delaminated region because of the lower thickness values. As the frequency becomes higher, the group velocity curves of two modes reach the same values (c_l) in the un-delaminated region.

The magnitudes and phases of reflection and transmission coefficients versus dimensionless frequency are shown in Figs. 4–9 for a given delaminated position $h_1/h = 0.4$. The left vertical axes denote the magnitudes while right vertical axes denotes the phases. Both open and closed delaminations are considered in these figures. Sub-figures (a) and (b) describes the modes transmitted and converted from the first and second flexural incident waves, respectively.

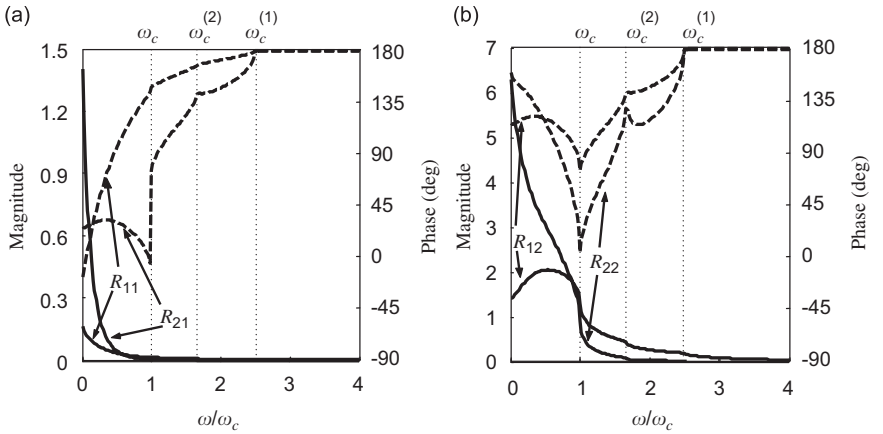

Fig. 5. Reflection coefficients (R_{jk}, for j, $k = 1,2$) ($h_1/h = 0.4$) under closed delamination condition (solid line: magnitude; dotted line: phase). Wave reflection from (a) first flexural mode and (b) second flexural mode.

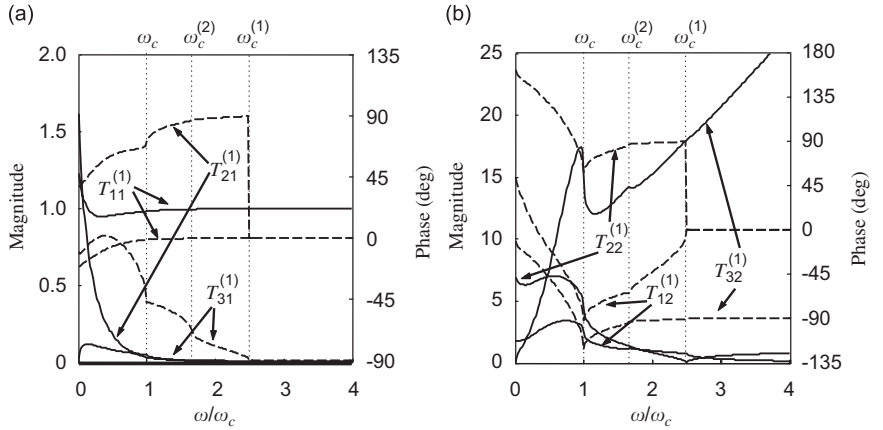

Fig. 6. Magnitudes and phases of transmission coefficients ($T_{jk}^{(1)}$, for $j = 1,2,3$, $k = 1,2$) in upper sub-beam ($h_1/h = 0.4$) under open delamination condition (solid line: magnitude; dotted line: phase). Wave transmission from (a) first flexural mode and (b) second flexural mode.

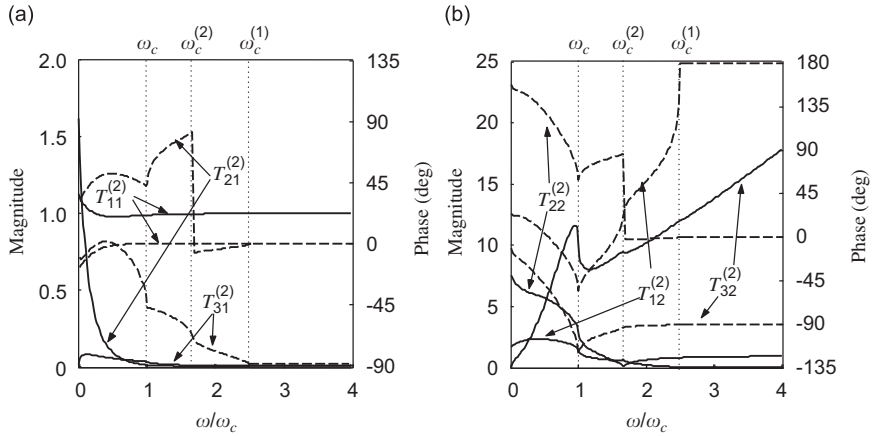

Fig. 7. Magnitudes and phases of transmission coefficients ($T_{jk}^{(2)}$, for $j = 1,2,3$, $k = 1,2$) in lower sub-beam ($h_1/h = 0.4$) under open delamination condition (solid line: magnitude; dotted line: phase). Wave transmission from (a) first flexural mode and (b) second flexural mode.

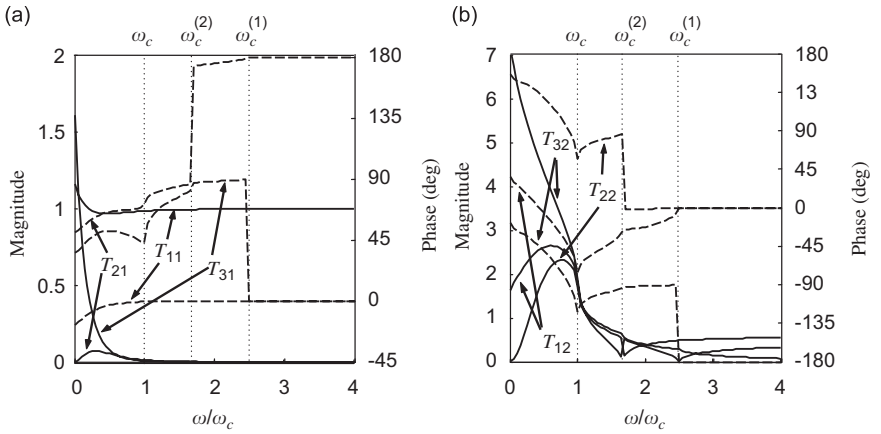

Fig. 8. Magnitudes and phases of three flexural transmission coefficients (T_{jk}, for $j = 1,2,3$, $k = 1,2$) in delaminated region ($h_1/h = 0.4$) under closed delamination condition (solid line: magnitude; dotted line: phase). Wave transmission from (a) first flexural mode and (b) second flexural mode.

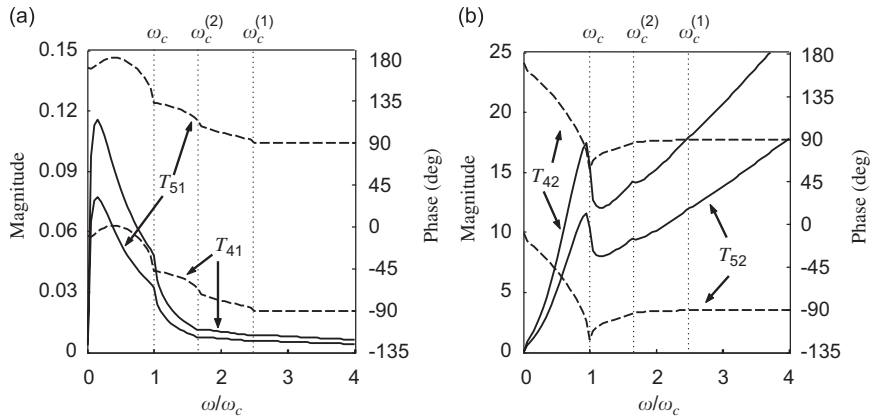

Fig. 9. Magnitudes and phases of two extensional transmission coefficients (T_{jk}, for $j = 4,5$, $k = 1,2$) in delaminated region ($h_1/h = 0.4$) under closed delamination condition (solid line: magnitude; dotted line: phase). Wave transmission from (a) first flexural mode and (b) second flexural mode.

It is clearly seen by comparing Figs. 4 and 5 that, as expected, the reflection coefficients are very insensitive to the delaminated surface conditions. The reflection magnitude (reflectivity) monotonically deceases as frequencies increase except $|R_{12}|$, where the reflection starts to increase and then decrease after $\omega/\omega_c = 0.6$. In the lower frequency domain, where the frequency is below the cut-off frequency in the un-delaminated region, although the reflection coefficient $|R_{21}|$ has larger magnitude, the wave is non-propagating evanescent type and decays exponentially from the delamination tip. When the excitation source contains the second propagating mode, $|R_{12}|$ and $|R_{22}|$ decrease rapidly near ω_c. The phases of flexural reflection coefficients depend strongly on the frequency when $\omega < \omega_c^{(1)}$. The reflection coefficients $|R_{31}|$ and $|R_{32}|$ (not shown in the figures) are virtually zero and phases are shifted by 90°, implying that there is almost no extensional wave reflected from the two flexural modes. The induced extensional waves arise primarily from the self-equilibrating forces to ensure equilibrium between the sub-beams.

Since the two extreme delamination surface conditions involve different formulation and resulting different displacement fields, the transmission coefficients may vary between open and closed delaminations, which are shown in Figs. 6–9. Figs. 6 and 7 give the transmission coefficients of two sub-beams for open delamination surfaces, respectively; while Figs. 8 and 9 present the transmission coefficients of flexural and extensional modes under closed delamination surfaces, respectively. Comparing the curves among Figs. 6–9(a),

the coefficients strongly depend on the frequency in the frequency $\omega<\omega_c$; beyond this frequency, there is almost no mode conversion, i.e., $|T_{n1}|\approx 0$ ($n=2$–5); all the first flexural wave energy directly transmits from the un-delaminated region into the delaminated region, i.e., $|T_{11}|\approx 1$. Comparatively, the coefficients converted from the second mode are much higher than the one converted from the first mode when $\omega<\omega_c$, but these modes involve no power transmission since the evanescent wave cannot transport the energy. And these coefficients vary rapidly with frequencies, especially at the cut-off frequency.

The coefficients of flexural modes converted from the second mode, such as $|T_{12}|$ and $|T_{22}|$ in Figs. 6(b) and 7(b), $|T_{12}|$, $|T_{22}|$ and $|T_{32}|$ in Fig. 8(b), are significantly reduced when the frequency is beyond the cut-off frequency ($\omega>\omega_c$). It should be noticed that the coefficients of extensional mode converted from the second mode, such as $|T_{32}|$ in Figs. 6(b) and 7(b), $|T_{42}|$, and $|T_{52}|$ in Fig. 9(b), increase with the varying frequency. This can be explained by the fact that the second flexural mode $\psi(x, t)$ introduces the rotation of the cross-section. This rotation induces large longitudinal motion in the sub-beams to maintain the rotation compatibility at the junction of the delamination tip.

Using the power flow expression in Eq. (41), the reflected and transmitted energies for both open and closed delamination surfaces are shown in Fig. 10. Numerical results based on the formulation show that the energy is conserved for all frequencies. In this study, two types of incident waves are chosen: $b=0$ (the first flexural wave mode only) and $b/a=1$ (two incident flexural waves have identical magnitudes). When $\omega>\omega_c$, the two cases (open and closed delamination) have very close results of the energy transmission and reflection ratios are almost independent of the delamination surface conditions. A notable difference in the energy transmission ratios occur in the lower frequency domain for these two delamination surface conditions. Moreover, there is a marked difference between Fig. 10(a) and (b) when $\omega>\omega_c$, because the second flexural mode is involved. And there is a high energy reflection when the frequency is just beyond the cut-off frequency ω_c shown in Fig. 10(b). This is because in this frequency domain the wave transmitting into the two sub-beams are evanescent, only one propagating mode transmitted into the delamination region. Thus all the energy of the second flexural mode is reflected back into the un-delaminated region.

The waves transmitted in the delamination region from the incident flexural waves experience mode conversion of the extensional wave and the flexural wave varying with the frequency can be obtained. Fig. 11 shows the transmitted energy ratios among various modes for different excitation frequencies. It can be concluded that the A_0 mode is converted most of the energy when the frequency is lower than the cut-off frequency in the un-delaminated region. While the frequency is beyond ω_c and $b=0$ (see Fig. 11(a)), which means there is no second incident mode, A_0 mode transmitted almost all of the energy, thus there is no mode conversion. When $\omega>\omega_c$ and $b/a=1$ (see Fig. 11(b)), portion of the transmitted energy is shared by the extensional mode. This suggests that the extensional motion in the two sub-beams is mostly converted from

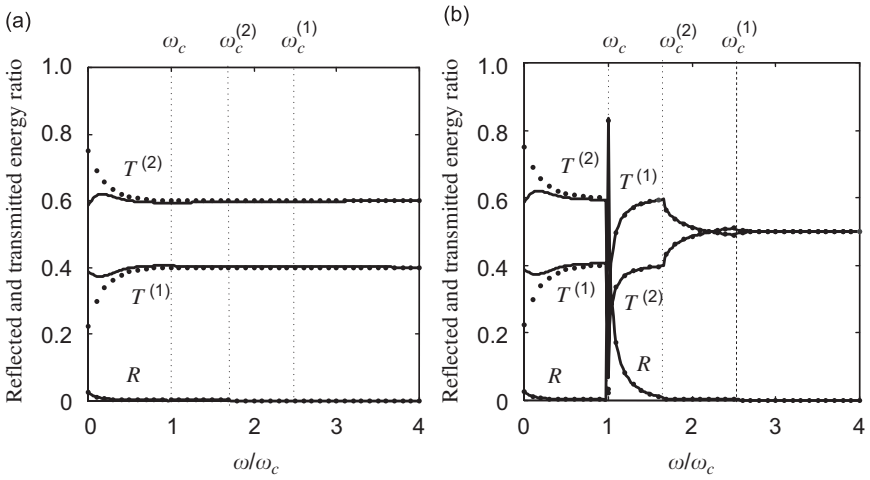

Fig. 10. Reflected energy ratio (R) and transmitted energy ratios ($T^{(i)}$, for $i=1,2$) ($h_1/h=0.4$) (solid line: open delamination; dotted line: closed delamination) (a) $b=0$; and (b) $b/a=1$.

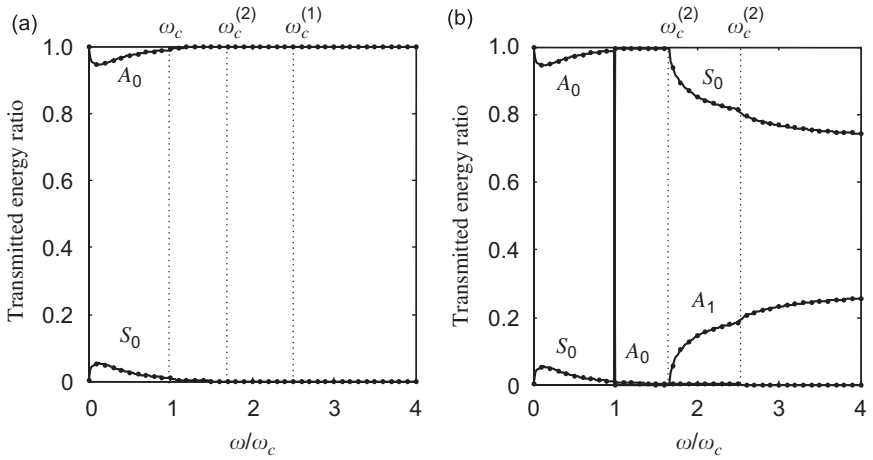

Fig. 11. Transmitted energy ratios among various wave modes (A_0, S_0, A_1) at $h_1/h = 0.4$ (solid line: open delamination; dotted line: closed delamination): (a) $b = 0$ and (b) $b/a = 1$.

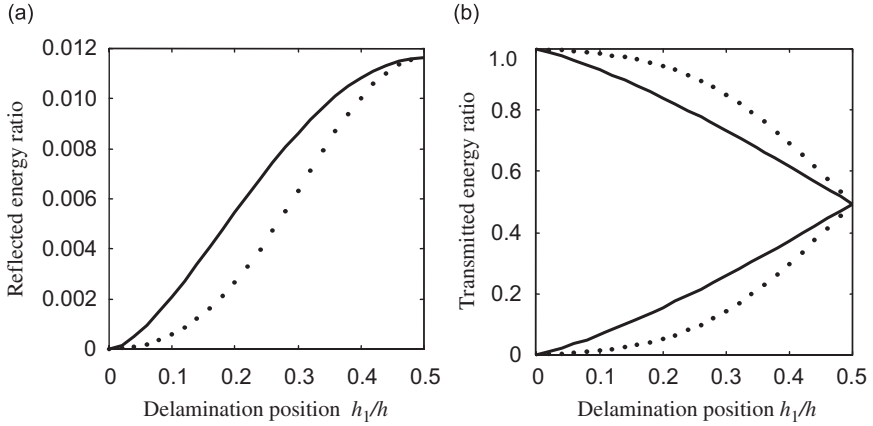

Fig. 12. Reflected energy ratio (R) and transmitted energy ratios ($T^{(i)}$, for $i = 1,2$) versus the delamination position ($\omega = 0.1\omega_c$): (a) reflected energy ratio and (b) transmitted energy ratio (solid line: open delamination; dotted line: closed delamination).

$\psi(x,t)$, rotation of the cross-section of the beam. The other flexural modes A_1 is present when the frequency is beyond the cut-off frequency of the sub-beam. In the all frequency domain, the transmitted energy of wave modes is insensitive to the delamination surface conditions.

Fig. 12 shows the effect of various delaminated positions in the thickness direction on the reflected and transmitted energy ratios at a given frequency $\omega = 0.1\omega_c$. At this frequency, the transmitted wave only contains S_0 and A_0 modes, and the energy ratios for extensional wave versus delamination position are shown in Fig. 13. The reflected energy ratios of two cases are slightly different when h_1/h is below 0.4, while matching well when h_1/h is close to 0.5. It is because the contact pressure will be larger when the delamination being more asymmetrical. Especially, in the case of symmetric delamination, i.e., $h_1/h = 0.5$, there is no contact pressure, and the results of two cases are identical. This reason is also true for the energy transmission ratios. Generally, the reflected energy increases as the delamination position is closer to the middle plane, and reaches maximum value at $h_1/h = 0.5$. This can be simply explained by the reduction of the bending stiffness in the delaminated region, the maximum occurring at $h_1/h = 0.5$. The energy ratio of the transmitted extensional mode increases monotonically with increase of h_1/h, and reach the maximum value at $h_1/h = 0.5$.

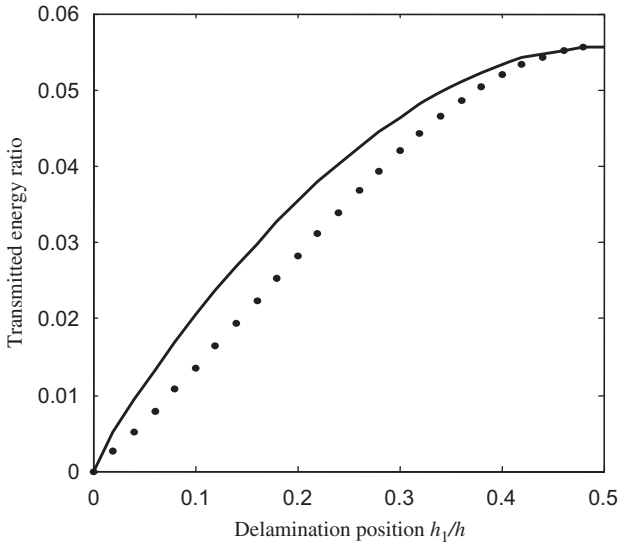

Fig. 13. Transmitted energy ratio (T^{S_0}) for extensional wave mode S_0 versus the delamination position ($\omega = 0.1\omega_c$) (solid line: open delamination; dotted line: closed delamination).

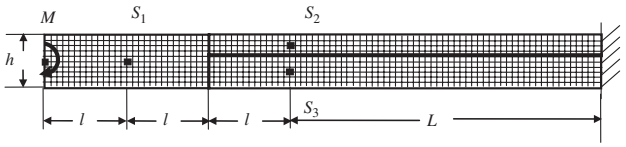

Fig. 14. The schematic of the beam modeled in using finite elements.

6. Comparison with results from finite element method

In order to verify the accuracy of the analytical method of power reflection and transmission in a semi-infinite delamination using the two extreme delaminated surface conditions, a finite element analysis using MSC software is conducted to model the wave propagation in the delaminated beam. The delaminated surfaces are modeled by gap elements that impose normal forces to avoid interpenetration on the portion of the delamination surfaces during the wave propagation. The true interface condition would probably involve frictional slippage and dissipation. Fig. 14 shows the schematic of the delaminated cantilever beam with the geometry: $l = 150$ mm, $L = 550$ mm, and $h = 1.8$ mm. Sensor S_1 located at middle plane of the un-delaminated region is used to measure the incident wave and reflected wave. Sensors S_2 and S_3 at the middle plane of two sub-beams are used to measure the transmitted wave, respectively. It should be noticed that S_2 and S_3 contain both transverse and longitudinal displacements at the middle plane, while S_1 only contains the transverse displacement. The element is chosen by a plane strain 4-node rectangular element. Note that the size of each element depends on the frequency of the guided wave. It must be satisfied that there are more than 8 elements in a wavelength to minimize the numerical distortion.

Sections 3 and 4 discussed the (power) reflection and transmission incident upon the delamination of harmonic flexural waves of a single frequency. In practice it is unlikely to generate a single frequency wave in limited time duration, in this section a narrowband incident wave is excited to examine the interaction of flexural waves with delamination using finite element method. Thus, a Fourier integral is needed to calculate the wave response. The incident flexural wave is generated at the left of the cantilever beam by exciting a concentrated moment at the middle node of the left end of the beam, which can be mathematically described by

$$M(t) = M_0[H(t) - H(t - 5/f_0)]\left(1 - \cos\frac{2\pi f_0 t}{5}\right)\sin 2\pi f_0 t. \tag{44}$$

This wave packet denotes a five-peaked narrowband signal modulated by a Hanning window, which the wave energy is concentrated around the central frequency f_0. The excitation signal is chosen, such that the central frequency is 50 kHz (approximately 0.1 of the cut-off frequency f_c). This signal has no significant energy above the cut-off frequency of the A_1 mode, thus only first the flexural mode is excited. The wave transmitted displacement will be firstly generated at the left end of the beam, described as $a_0(t)$. In this linear transient wave analysis, the wave propagates at the same frequency content of the applied excitation signal. The frequency spectrum of the transient wave displacement can be obtained using Fourier transform and can be written as

$$A_0(\omega) = \int_{-\infty}^{+\infty} a_0(t)\, \mathrm{e}^{-\mathrm{i}\omega t}\, \mathrm{d}t. \tag{45}$$

The magnitudes of wave packets received by three sensors in frequency domain could be obtained by multiplying the reflection and transmission coefficients on incident wave packet. Meanwhile, there is phase-shift caused by the wave propagation distance shown in Fig. 14. This would be also multiplied on the incident wave. Then the signal received by each sensor is the superposition of the incident and scattered wave including transmission and reflection (if any) waves:

$$A_{S_1}(\omega) = A_0(\omega)\, \mathrm{e}^{\mathrm{i}k_1 l} + R_{11} A_0(\omega)\, \mathrm{e}^{3\mathrm{i}k_1 l}, \tag{46a}$$

$$A_{S_2}(\omega) = T_{11}^{(1)} A_0(\omega)\, \mathrm{e}^{2\mathrm{i}k_1 l + \mathrm{i}k_1^{(1)} l}, \quad C_{S_2}(\omega) = T_{31}^{(1)} A_0(\omega)\, \mathrm{e}^{2\mathrm{i}k_1 l + \mathrm{i}k_e l}, \tag{46b}$$

$$A_{S_3}(\omega) = T_{11}^{(2)} A_0(\omega)\, \mathrm{e}^{2\mathrm{i}k_1 l + \mathrm{i}k_1^{(2)} l}, \quad C_{S_3}(\omega) = T_{31}^{(2)} A_0(\omega)\, \mathrm{e}^{2\mathrm{i}k_1 l + \mathrm{i}k_e l}, \tag{46c}$$

where $A_{S_1}(\omega)$, $A_{S_2}(\omega)$ and $A_{S_3}(\omega)$ denote the flexural signals received by S_1, S_2, and S_3, respectively, and $C_{S_2}(\omega)$ and $C_{S_3}(\omega)$ represent the extensional signals received, respectively, by S_2 and S_3. For example, $A_{S_1}(\omega)$ consists of incident wave and reflected wave. The incident wave propagating to S_1 experiences a phase shift by a distance l and the reflected wave by $3l$. Since both waves propagate in the un-delaminated region, a single wavenumber k_1 is used.

Then the signal in the time domain can be symbolically represented by using its inverse Fourier transform shown as follows:

$$a(t) = \frac{1}{2\pi} \int_{-\infty}^{\infty} A(\omega)\, \mathrm{e}^{\mathrm{i}\omega t}\, \mathrm{d}\omega, \tag{47}$$

where $A(\omega)$ represents $A_{S_1}(\omega)$, $A_{S_2}(\omega)$, $A_{S_3}(\omega)$, $C_{S_2}(\omega)$, and $C_{S_3}(\omega)$ for brevity, $a(t)$ is the signal in time domain, respectively. The numerical results of symmetric delamination case, leading to the maximum reduction of bending stiffness, are presented for this example. The signals received from the finite element method nodes compared with analytical results (open delamination) are shown in Fig. 16. The analytical results chosen from open delamination case have a good agreement with the finite element method. As a result of symmetric status, signal received by S_3 is the same as S_2, so it is only shown the signals received by S_1 and S_2 for brevity.

In order to make a convenient comparison, the signals are non-dimensionalized according to incident wave. Fig. 15(a) denotes the incident wave packet passing by associated with reflected wave packet. A good agreement can be seen between finite element method model and theory and the magnitudes of the reflected wave are both about 0.1. The transmitted wave contains both flexural wave and extensional wave in S_2 mode, so Fig. 15(b) and (c) shows both of the signals. The signals obtained by two methods match well. Moreover, the extensional wave reaches at position S_2 earlier than the flexural wave. This is because there is a length of distance l to be propagated by the transmitted wave, and the extensional wave speed is about six times of the flexural wave according the material in this paper. There are additional wave packets in transmitted extensional waves of finite element method results in Fig. 15(c), which is the extensional wave reflected from the right boundary of the cantilever beam.

For the dispersive phenomenon, the whole power flow of the analytical method is still needed to consider all the components in the whole frequency domain. Thus, the power flow can be written as

$$\langle P \rangle = \frac{1}{4\pi^2} \int_{-\infty}^{\infty} \lambda(\omega) \left| A(\omega) \right|^2 \mathrm{d}\omega, \tag{48}$$

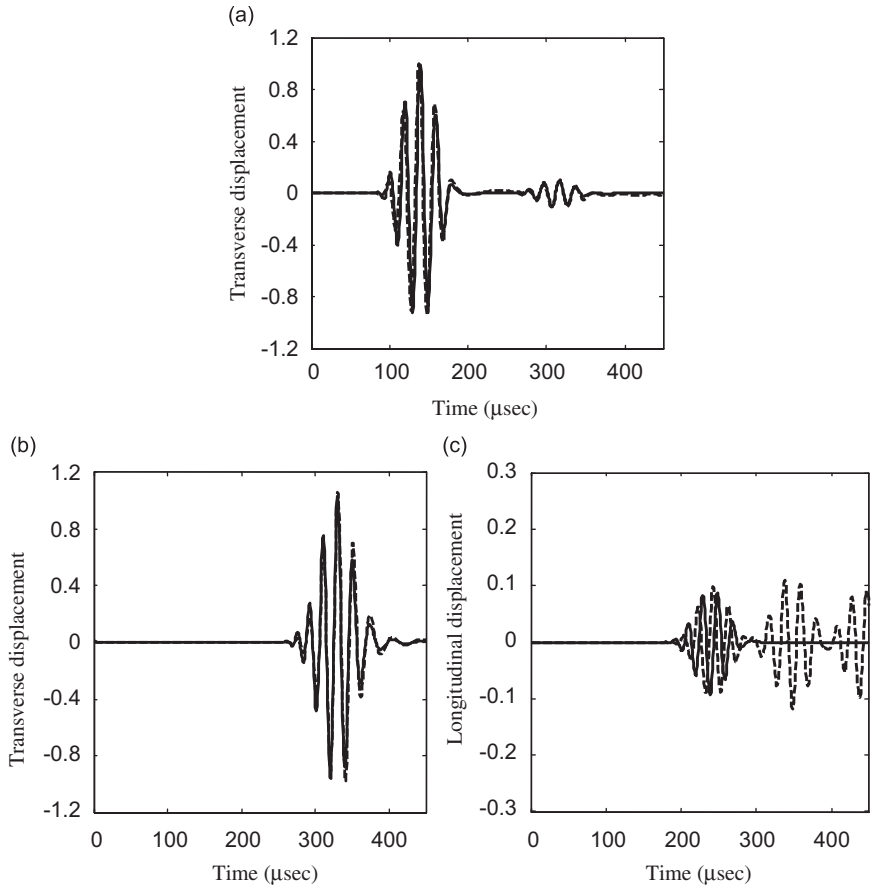

Fig. 15. The signals received from the finite element method nodes compared with analytical results (open delamination): (a) transverse displacement at S_1; (b) transverse displacement at S_2; (c) longitudinal displacement at S_2 (solid line: Timoshenko beam theory; dotted line: finite element method).

where $\lambda(\omega)$ can be considered as the coefficient of the power flow dependent on frequency, while $A(\omega)$ is the transverse displacement magnitude of the transient wave packet by spectral description. The reflected energy ratio and transmitted energy ratio for each mode could be calculated according to Section 4 together with the integral in the frequency domain as Eq. (48).

As the finite element method model is based on the elastic beam theory, the expression of power flow is different from Timoshenko theory given by Eq. (36), and it can be written as follows:

$$\langle P\rangle = -\frac{1}{t_0}\int_0^{t_0}\int_{-h/2}^{h/2}(\sigma_x\dot{u} + \tau_{xz}\dot{w})\,\mathrm{d}z\,\mathrm{d}t, \tag{49}$$

where the stresses σ_x, τ_{xz} and displacements u, w are functions of coordinate x, z and time t. In order to calculate the power flow through the section y–z plane, the value of x is chosen as a constant x_0 arbitrarily. As the plane strain problem is discussed in this paper, these variables can be obtained at the nodes of the finite element method model with different coordinate z. Substituting the following Fourier transform of these variables, the power flow can be rewritten as

$$\langle P\rangle = -\frac{1}{8\pi^2}\int_{-h/2}^{h/2}\int_{-\infty}^{\infty}\mathrm{i}\omega[(\tilde{\sigma}_x\tilde{u} - \overline{\tilde{\sigma}}_x\overline{\tilde{u}}) + (\tilde{\tau}_{xz}\tilde{w} - \overline{\tilde{\tau}}_{xz}\overline{\tilde{w}})]\,\mathrm{d}\omega\,\mathrm{d}z, \tag{50}$$

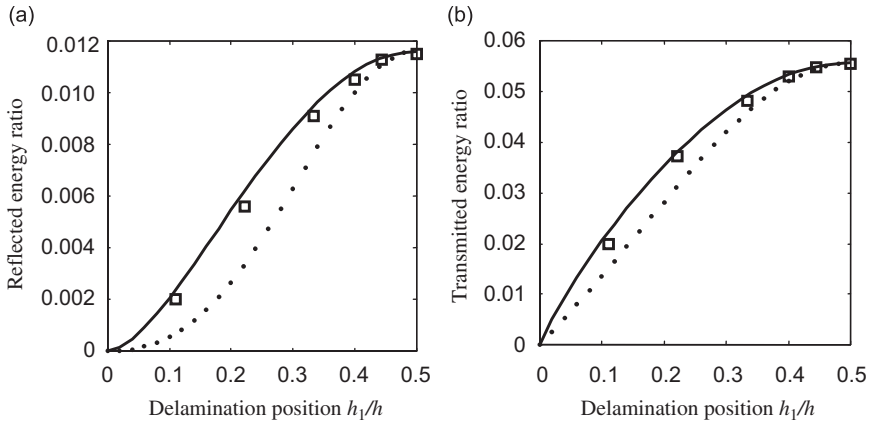

Fig. 16. (a) Reflected energy ratio and (b) transmitted energy ratio for extensional wave S_0 power versus different positions of the delamination (solid line: open delamination; dotted line: closed delamination; square symbol: finite element method).

where $\overline{\tilde{\sigma}}_x$, $\overline{\tilde{u}}$, $\overline{\tilde{\tau}}_{xz}$ and $\overline{\tilde{w}}$ denote the complex conjugates of $\tilde{\sigma}_x$, $\tilde{u}$, $\tilde{\tau}_{xz}$ and $\tilde{w}$. As the finite element method involves the discontinuity in the coordinate z, the integration in the thickness direction can be obtained by summation of the values in each node.

According to Eqs. (48) and (50), the reflected energy ratio of both analytical method (open and closed delamination) and the finite element method can be obtained by varying the position of the delamination, reflected energy ratio and transmitted energy ratio for extensional wave S_0 power are monotonically increasing with the depth of the delamination as shown in Fig. 16.

It can be concluded from the figures that the results using the finite element method are between two extreme delaminated surface conditions cases using analytical results, and are closer to the open delamination in both the reflected energy and the transmitted energy ratio for extensional wave S_0 power. Although the open delamination leads to overlapping between two surfaces in the analytical model, it provides better prediction than that of the delaminated surface being completely closed. The maximum reflected energy and maximum transmitted energy of extensional wave occur when the delamination occurs at the midplane, where the maximum shear stress for the A_0 mode is largest.

7. Conclusions

Wave reflection and transmission in composite beams containing a semi-infinite delamination is presented using Timoshenko theory for two extreme delaminated surface conditions: open delamination and closed delamination, respectively. The flexural wave reflection and transmission coefficients depend strongly on the frequency of the incident flexural waves as well as the position of the delamination. And they also reveal the mode conversion among two flexural wave modes and one extensional wave mode. The power distribution of the transmitted wave among modes provides a physical significance of mode conversion varying with the frequency. In addition, numerical results show the conservation of power transport in the whole frequency domain, which means the energy of incident wave transfers entirely to the energy of reflection wave and transmission wave. This is also used to verify the validity of the analytical method. The analytical results also give a good agreement with the simulation results from finite element analysis, which provide an efficient method of localizing the delamination in the thickness direction.

Acknowledgments

This research is partially supported by the National Natural Science Foundation of China under Grant nos. 50478037 and 10572058. Dr. Yuan would like to appreciate the support from the National Science Foundation Grant no. CMMI-0654233.

References

[1] J.T.S. Wang, Y.Y. Lou, J.A. Gibby, Vibration of split beams, *Journal of Sound and Vibration* 84 (1982) 491–502.
[2] P.M. Mujumdar, S. Suryanarayan, Flexural vibrations of beams with delaminations, *Journal of Sound and Vibration* 125 (1988) 441–461.
[3] J.J. Tracy, G.C. Pardoen, Effect of delamination on the natural frequencies of composite laminates, *Journal of Composite Materials* 23 (1989) 1201–1215.
[4] S.H.D. Valdes, C. Soutis, Delamination detection in composite laminates from variations of their modal characteristics, *Journal of Sound and Vibration* 228 (1999) 1–9.
[5] T.N. Farris, J.F. Doyle, Wave propagation in a split Timoshenko beam, *Journal of Sound and Vibration* 130 (1989) 137–147.
[6] N. Guo, P. Cawley, The interaction of lamb waves with delaminations in composite laminates, *Journal of Acoustical Society of America* 94 (1993) 2240–2246.
[7] E.A. Birt, Damage detection in carbon-fibre composites using ultrasonic Lamb waves, *Insight* 40 (1998) 335–339.
[8] T. Hayashi, K. Kawashima, Multiple reflections of Lamb waves at a delamination, *Ultrasonics* 40 (2002) 193–197.
[9] W. Ostachowicz, M. Krawczuk, M. Cartmell, M. Gilchrist, Wave propagation in delaminated beam, *Computers and Structures* 82 (2004) 475–483.
[10] Y. Lase, M.N. Ichchou, L. Jezequel, Energy flow analysis of bars and beams: theoretical formulations, *Journal of Sound and Vibration* 192 (1996) 281–305.
[11] J. Pan, R. Ming, Colin H. Hansen, R.L. Cark, Experimental determination of total vibratory power transmission in an elastic beam, *Journal of Acoustic Society of America* 104 (1998) 898–906.
[12] J. Bazer, R. Burridge, Energy partition in the reflection and refraction of plane waves, *SIAM Journal of Applied Mathematics* 34 (1978) 78–92.
[13] C.H. Wang, L.R.F. Rose, Wave reflection and transmission in beams containing delamination and inhomogeneity, *Journal of Sound and Vibration* 264 (2003) 851–872.
[14] J.M. Whitney, *Structural Analysis of Laminated Anisotropic Plates*, Technomic Publishing Co. Inc., Lancaster, PA, 1987.
[15] J.D. Achenbach, *Wave Propagation in Elastic Solids*, North-Holland Publishing Company, Amsterdam, 1984.